공학석사학위논문

저온 고체산화물 연료전지를 위한 니켈기반 박막 연료극의 제작 및 전기화학적 특성 분석

Fabrication and Electrochemical Performance Characterization of Nickel-based Thin-film Anodes for Low-temperature Solid Oxide Fuel Cells

2017 년 02 월

서울대학교 대학원

기계항공공학부

이 예 근

Abstract

Fabrication and Electrochemical Performance Characterization of Nickel-based Thin-film Anodes for Low-temperature Solid Oxide Fuel Cells

Yeageun Lee

Department of Mechanical and Aerospace Engineering

Seoul National University

In this study, various types of pure nickel (Ni) and Ni-based cermet anodes were fabricated onto nanoporous substrates and applied to thin-film solid oxide fuel cells (SOFCs) for low temperature operation. Sputtering technique was utilized to fabricate the experimental fuel cells by sequential deposition of anodes, electrolytes, and cathodes on the substrate materials.

Depending on its nanostructure, the pure Ni anodes exhibited comparable performance to the optimized platinum (Pt)

anode at 500 ℃. However, compared to the optimized Pt anode cell, the polarization resistances of the pure Ni anode cells were significantly larger.

In order to reduce the polarization resistance of Ni-based anodes and obtain better electrochemical characteristics, a Ni/Ni-based cermet bilayer anode structure was introduced. For optimization of the Ni-based cermet, five types of Ni-yttria stabilized zirconia (Ni-YSZ) composite films were fabricated via co-sputtering method and electrochemically investigated. As a result, a Ni-YSZ film fabricated by co-sputtering method with 50 W DC and 100 W RF powers showed the lowest polarization resistance. Therefore, this Ni-YSZ film was selected as Ni-YSZ layer of the Ni/Ni-YSZ bilayer anode. For Ni layer, a 150 nm-thick pure Ni anode, which showed the best performance among the fabricated pure Ni films, was employed. This 150 nm-thick pure Ni film was sputtered with DC 200 W under 5 mTorr argon (Ar) atmosphere.

On the nanoporous substrate, the Ni-based bilayer anode, YSZ electrolyte, and Pt cathode was sequentially deposited to fabricate a full cell. At 500 ℃, the peak power density of the full cell was about 37 % higher (282 mW/cm^2) than that of the

optimized Pt anode cell (205 mW/cm^2). Moreover, the Ni-based bilayer anode cell exhibited much lower ohmic and polarization resistances compared to other fabricated cells. This shows the acceptability of non-noble metal anode for low-temperature SOFCs.

Keyword : solid oxide fuel cell (SOFC), thin film, low temperature, Ni-YSZ, co-sputtering

Student Number : 2014-21866

Contents

List of Tables

List of Figures

* Contents in this thesis will be published in the international journal.

Chapter 1. Introduction

1.1. Study Background

1.1.1. Fuel Cells

During the last decades, the Earth suffered from the rapid industrialization. To achieve and maintain developed industries, an immense amount of resources, e.g. fossil fuels, has been exploited indiscriminately by human beings to generate sufficient energy. As a result, serious environmental problems such as global warming, air pollution, and desertification have occurred. These issues directly affect the quality of human life negatively. Therefore, scientists and engineers started to find out renewable energies for better sustainability.

Among the several candidates, hydrogen energy has a high potential of becoming the major energy source, since the hydrogen is one of the most common elements in the Earth and can be obtained from various resources.[1,2] However, to use it as a clean energy source, further investigation is required.

Fuel cells have been considered as promising energy conversion devices in utilizing hydrogen fuel. A single fuel cell has three basic components: anode, electrolyte, and cathode. In the anode side, one hydrogen molecule breaks into two hydrogen ions and two electrons. These electrons travel to the external circuit to provide electricity. In the cathode side, on the other hand, one oxygen molecule gets four electrons and becomes two oxygen ions. Then, these oxygen ions pass through the electrolyte and meet hydrogen ions at the anode/electrolyte interface to produce water as exhaust.[3]

Anode: $2H_2 + 2O^{2-}(from\ cathode) \rightarrow 2H_2O + 4e^-$

Cathode: $O_2 + 4e^- \rightarrow 2O^{2-}$

Overall: $2H_2 + O_2 \rightarrow 2H_2O$

Depending on the electrolyte materials, hydrogen ions can also travel to the cathode/electrolyte interface. In this case, water is produced on the cathode side. Since there is no other product besides water in the whole process, we can get electricity eco-friendly. Figure 1.1 illustrates the basic concept of the fuel cells.

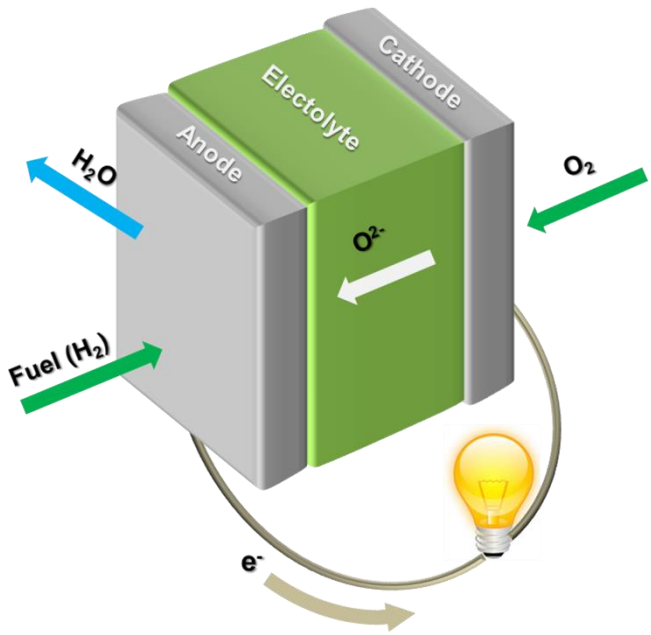

Figure 1.1 Basic concept of fuel cells.

1.1.2. Solid Oxide Fuel Cells

There are various types of fuel cells usually named after their electrolyte materials. Table 1.1 shows the major fuel cells and their detailed information.[3] (PEMFC: polymer electrolyte membrane fuel cell, *also known as* proton exchange membrane fuel cell, PAFC: phosphoric acid fuel cell, AFC: alkaline fuel cell, MCFC: molten carbonate fuel cell, SOFC: solid oxide fuel cell)

Table 1.1 Fuel cell types.[3]

	PEMFC	PAFC	AFC	MCFC	SOFC
Electrolyte	Polymer membrane	Liquid H_3PO_4	Liquid KOH	Molten carbonate	Ceramic
Charge carrier	H^+	H^+	OH^-	CO_3^{2-}	O^{2-}
Operating temperature	80 ℃	200 ℃	60–220 ℃	650 ℃	600–1000 ℃
Fuel compatibility	H_2, methanol	H_2	H_2	H_2, CH_4	H_2, CH_4, CO

Among the aforementioned fuel cell types, SOFCs have superiority in fuel flexibility and simplicity of subsystems.[4,5] Moreover, we can utilize low-cost materials like nickel (Ni) as catalysts for SOFCs. However, as written on the Table 1.1, SOFCs generally operate at extremely high temperature, around 800 ℃, to have sufficient ionic conductivity throughout their solid oxide electrolytes. Figure 1.2 illustrates the ionic conductivities of the most common SOFC electrolyte materials, 8 mol % of yttria stabilized zirconia (YSZ)[6–8] and 0.1 gadolinium doped ceria ($Ce_{0.9}Gd_{0.1}O_2$, GDC), in air.[6,9–13]

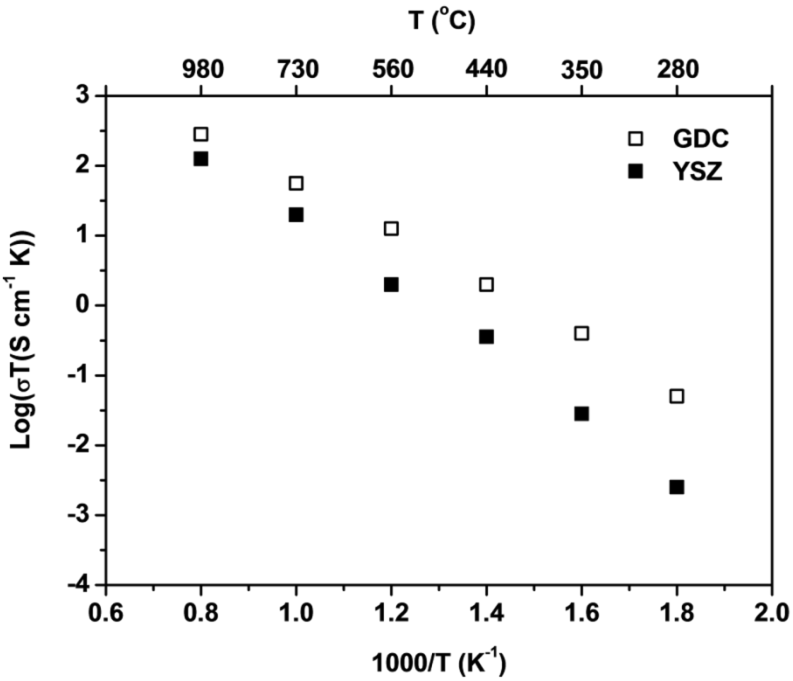

Figure 1.2 Ionic conductivity of 8 mol % YSZ and 0.1 GDC in air.[6–13]

As shown in Figure 1.2, the ionic conductivities of the solid oxides significantly increase as the temperature rises. Considering that the electrolyte thicknesses of the conventional SOFCs range from several to tens of micrometers[14,15], the operating temperature lower than 600 ℃ makes solid oxide electrolytes have poor oxygen ion transfer capability. For example, based on the data from Figure 1.2, a 20 μm-thick YSZ electrolyte gives approximately 1.5 $\Omega \cdot cm^2$ of ohmic resistance to a single cell at 500 ℃, while it gives even less than 0.1 $\Omega \cdot cm^2$ of ohmic resistance to the cell at 800 ℃.

Typically, the ohmic resistance from the electrolyte must not exceed 0.15 $\Omega \cdot cm^2$ for proper operation.[15]

Although the high operating temperature is beneficial for the ion conductivity and catalytic activity of SOFCs, it induces serious disadvantages: long start-up time, narrow applications, limitation in material selection, sealing problem, and thermal instability.[16-18] In order to overcome these issues, researchers have devoted to reduce the operating temperature of SOFCs.

1.1.3. Thin-film SOFCs

There are two major barriers in reducing the operating temperature of SOFCs. One is lowered ionic conductivity of electrolytes, and the other is decreased catalytic activity of electrodes. Both the ionic conductivity and catalytic activity of SOFCs decrease as the temperature reduces.[3]

Lowered ionic conductivity, however, can be compensated by thinning the electrolytes. With various thin film techniques such as sputtering, pulsed laser deposition (PLD), atomic layer deposition (ALD), and plasma enhanced atomic layer deposition

(PEALD), even less than 1 μm-thick electrolytes have been successfully fabricated.[14,19-27] Then, free-standing structures[14,22-25] and nanoporous substrates[26-31] have employed to produce full cells with those nanoscale electrolytes. Schematics of the both thin-film SOFC types are illustrated in Figure 1.3. The produced full cells operated properly at 350~500 ℃ with a good gas tightness.

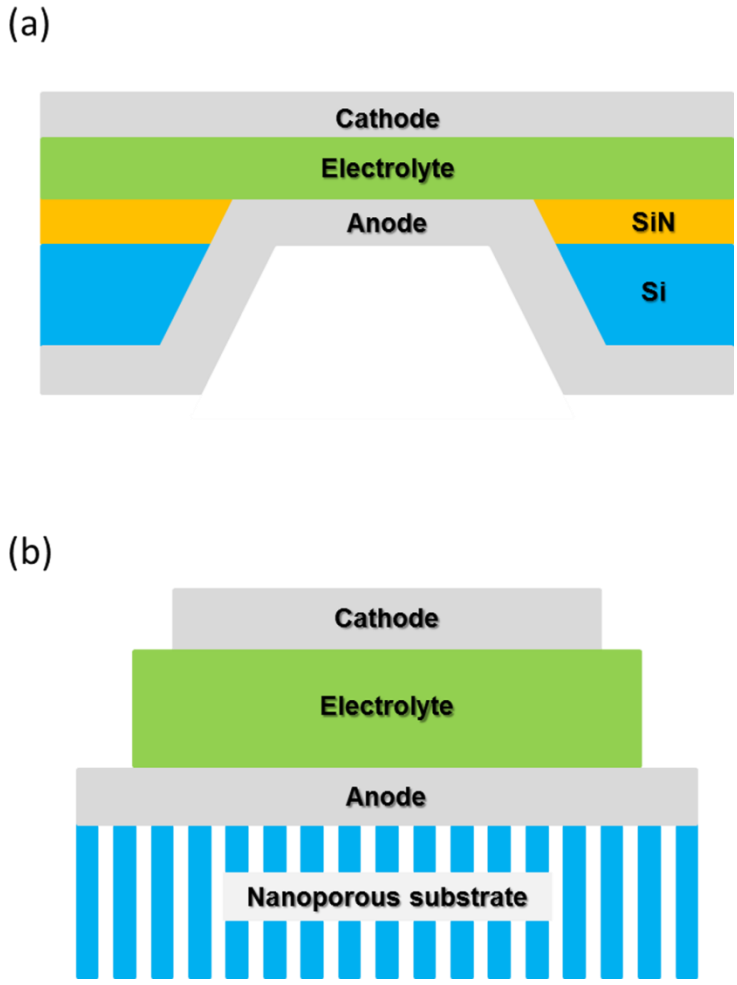

Figure 1.3 Schematics of SOFCs supported by (a) free-standing structure and (b) nanoporous substrate.

1.2. Purpose of Research

In spite of the introduction of thin-film SOFCs, the decreased catalytic activity at low temperature has not been fully overcome. Ni has been widely utilized as an anode material for traditional SOFCs, but its catalytic activity for hydrogen evolution/oxidation reaction (HER/HOR) is inferior to that of platinum (Pt)[32-35] and insufficient at the reduced temperature. As a result, Pt has been used as an alternative anode material for low-temperature SOFCs operating below 500 ℃. However, the high material cost of Pt imposes another barrier for commercialization of low-temperature SOFCs.

Besides introducing highly active catalyst materials, optimizing the anode nanostructure to have favorable characteristics for HOR can also significantly improve the electrochemical properties.[36,37] For example, electrons produced at the anode/electrolyte interfaces mostly travel in the lateral direction of the anode film to reach the external circuit.[38,39] Therefore, the thicker layer, and thus the larger cross-sectional area, would be advantageous for reducing ohmic resistance resulting from electronic conduction. However, it is also possible that the thicker

layer has an adverse effect on fuel diffusion to the reaction sites. Especially for thin-film SOFCs fabricated onto nanoporous anodic aluminum oxides (AAOs), the thicker anode can considerably block the pores from AAO and impede the formation of triple phase boundaries (TPBs) where the reaction occurs.[28] In addition, the porosity of the anode could influence the sheet resistance, fuel diffusion, and surface morphology of the anode. The more porous structure may provide the narrower path for electrons with the higher sheet resistance, while it provides the wider path for gas molecules with the efficient fuel supply. Therefore, modified electrode structures can be solutions for compensating the reduced catalytic activity. Furthermore, in low temperature operation, changes in the anode structure significantly affects not only anodic catalytic activity but also the total performance of the fuel cell.[40] Consequently, examining various anode structures with low-cost materials would give insight into the possibility of substituting the precious catalysts.

In this study, pure Ni and Ni-based composite anodes were demonstrated as replacements of Pt-based anodes, all of which are fabricated by sputtering. The pure Ni anodes were fabricated under various conditions and electrochemically compared with those of the

Pt anodes. Although the peak power densities showed by some Ni anodes were acceptable for low temperature applications, they needed further improvement in order to compete with the Pt anodes. Therefore, we decided to enlarge the reaction sites with an additional Ni-YSZ cermet layer. By inserting the Ni-YSZ layer between the Ni anode and YSZ electrolyte, the peak power density of the cell was enhanced from 196 mW/cm^2 to 282 mW/cm^2, which is more than 37 % higher than that of the optimized Pt anode cell. We expect that our anode structure would be widely utilized for low-temperature SOFCs, since Ni is one of the cheapest anode materials available in market today.

.

Chapter 2. Experimental Details

2.1. Fabrication of Experimental Cells

AAOs were utilized as substrates to support thin film SOFC structures. On the AAO template, anode, electrolyte, and cathode layers were deposited sequentially. The schematic of the fabricated cell is same as Figure 1.3(b).

All experimental cells have their own anode structure, and the fabrication processes of those anodes are written in section 2.2. For the electrolytes, an $Y_{16}Zr_{84}$ alloy target was utilized to deposit 600 nm-thick YSZ layers with 200 W RF sputtering under 5 mTorr of Argon (Ar) /O_2 (8:2) atmosphere. In case of the cathodes, 200 nm-thick Pt layers were deposited by 100 W DC sputtering under 90 mTorr of Ar atmosphere.

2.2. Fabrication of Various Anodes

2.2.1. Fabrication of the Optimized Pt Anode

From the previous work[28], a 450 nm-thick Pt film, which sputtered with 200 W DC power under 90 mTorr of Ar gas, showed the best performance as an anode layer among the various Pt films. Therefore, we simply employed this optimized Pt anode structure to this research. The detailed methodology of the optimization is available elsewhere.[28]

2.2.2. Fabrication of Pure Ni Anodes

We fabricated four different Ni anodes under various conditions by sputtering methods. In order to make differences in the porosity of the films, 5 mTorr and 90 mTorr of Ar atmosphere were applied. Under each atmosphere, 150 and 450 nm-thick Ni films were sputtered with 200 W DC power. Usually, more porous structure is fabricated under higher chamber pressure.[41,42] The sputtered Ni

films in this study also followed this tendency. Figure 2.1 shows the field emission secondary electron microscope (Fe-SEM) images of the fabricated Ni films. Clearly, the films deposited under 90 mTorr contain more voids and have more porous structures than the films deposited under 5 mTorr. Therefore, we named each Ni film as Ni-D(dense)-150, Ni-D-450, Ni-P(porous)-150, Ni-P-450. Table 2.1 summarizes the deposition conditions of the Ni films.

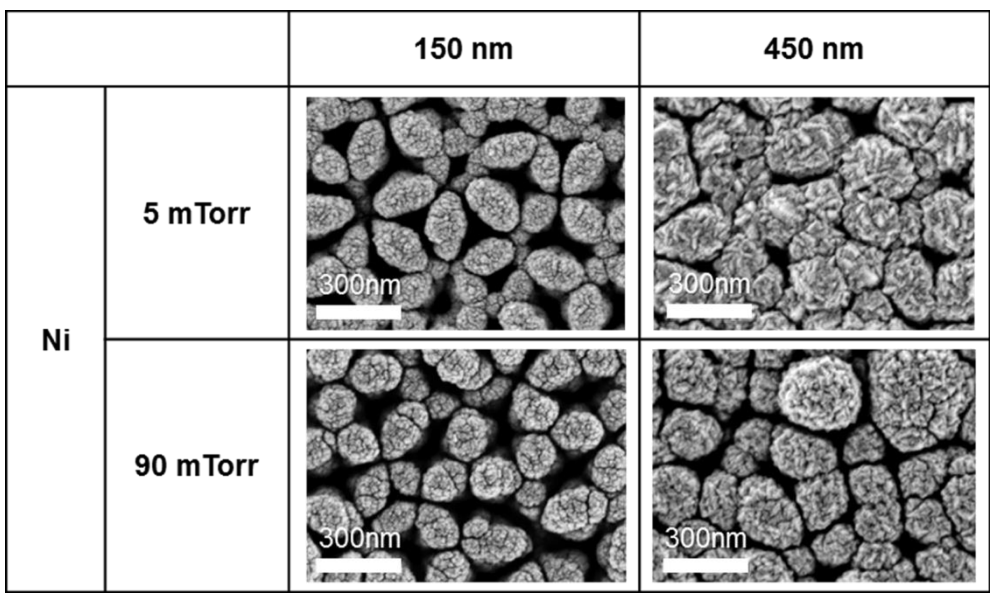

Figure 2.1 Surface morphologies of the fabricated Ni films.

Table 2.1 Deposition conditions of the various Ni anodes.

	Ni-D-150	Ni-D-450	Ni-P-150	Ni-P-450
Chamber pressure	Ar 5 mTorr	Ar 5 mTorr	Ar 90 mTorr	Ar 90 mTorr
Film thickness	150 nm	450 nm	150 nm	450 nm

The cross-sectional images, taken by a focused ion beam-scanning electron microscope (FIB-SEM), of the full cells with the pure Pt anode and the pure Ni anode are available in Figure 2.2.

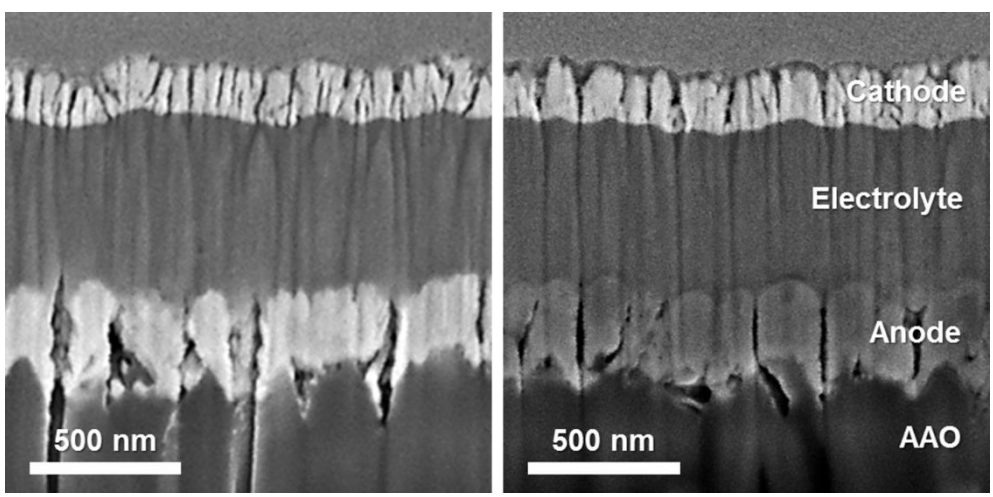

Figure 2.2 Cross-sectional images of (a) the pure Pt anode cell and (b) the pure Ni anode cell.

2.2.3. Fabrication of Ni-YSZ Cermet Anodes

By co-sputtering methods, we fabricated five Ni-YSZ films. All films were deposited under 5 mTorr of Ar/O_2 (8:2) mixture gas. During the fabrication processes, Ni was sputtered by 50 W DC power, and simultaneously, YSZ was sputtered by 200(NY1), 150(NY2), 100(NY3), 75(NY4), and 50(NY5) W RF power for each film to give different chemical composition to the films. The thicknesses of the films were fixed to 500 nm. Table 2.2 summarizes the deposition conditions of the Ni-YSZ films.

Table 2.2 Deposition conditions of the various Ni-YSZ films.

	NY1	NY2	NY3	NY4	NY5
Chamber pressure	Ar 5 mTorr				
Film thickness	500 nm				
DC power (for Ni)	50 W				
RF power (for YSZ)	200 W	150 W	100 W	75 W	50 W

2.2.4. Fabrication of a Ni/Ni-YSZ Bilayer Anode

In order to improve the electrochemical performance of the pure Ni anodes, a bilayer structure was introduced. On the AAO, a pure Ni layer, Ni-D-150, was deposited first. Then, Ni-YSZ cermet layer, 200 nm of NY3, was sputtered on the Ni-D-150 layer. The 600 nm-thick YSZ electrolyte and 200 nm-thick Pt cathode were also deposited sequentially. The schematic of the full Ni/Ni-YSZ bilayer anode cell is illustrated in Figure 2.3.

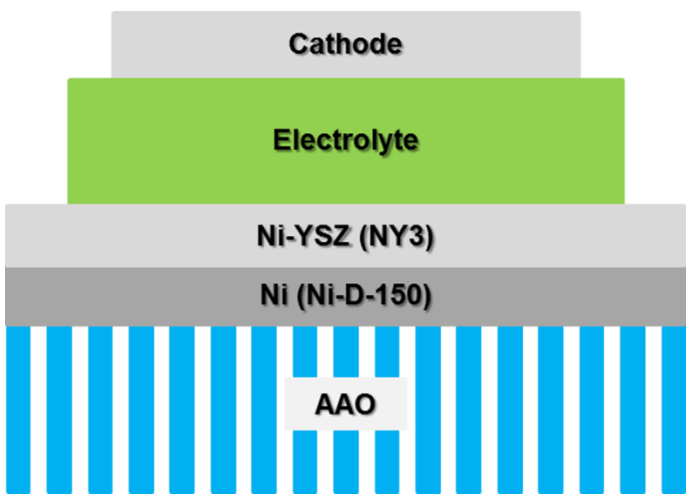

Figure 2.3 Schematic of the full Ni/Ni-YSZ bilayer anode cell.

2.3. Film and Cell Characterization

The fabricated cells were tested at 500 ℃ in our custom-made probe station. During the test, hydrogen was supplied to the anode chamber with a flow rate of 100 sccm, while the cathode was exposed to the ambient air. Detailed figure of the probe station is provided elsewhere.[38] Electrochemical impedance spectroscopy (EIS) data and current density-cell voltage curves (j-V curves) of the cells were plotted with a Solatron 1260/1287 system.

The surface morphologies of the anode films were examined with FE-SEM (Supra 40, Carl Zeiss), whereas the cross-sectional images of the cells were observed with FIB-SEM (Quanta 3D FEG, FEI Company).

The electrical conductivities of the Ni-YSZ films were measured by an automatic mapping four point probe resistivity measurement equipment (CMT-SR2000N) under room temperature.

Chapter 3. Result and Discussion

3.1. Investigating Various Pure Ni Anode Structures

In the previous work, the thick and porous Pt film exhibited the highest performance among the six types of Pt films.[28] Therefore, the porous Ni anodes, Ni-P-150 and Ni-P-450 which were deposited under 90 mTorr of Ar gas, were investigated first.

3.1.1. Porous Ni Anodes

In order to compare the electrochemical characteristics of the pure Ni anode cells to those of the cell utilizing highly active and precious material, Pt, the thin film SOFC with the thick and porous Pt anode (optimized Pt cell) was introduced.

Figure 3.1(a) illustrates the j-V and power density (j-V-P) curves of the cell with Ni-P-150, the cell with Ni-P-450, and the cell with the optimized Pt anode at 500 ℃. All three cells show approximately 1.1 V of open circuit voltages (OCVs), close to the

theoretical value of 1.15 V, indicating that the cells operate properly without any significant defect. However, the peak power densities of Ni-P-150 cell (96 mW/cm^2) and Ni-P-450 cell (149 mW/cm^2) were considerably lower than that of the optimized Pt cell (205 mW/cm^2). To find out the cause of the different performance, the impedance spectra of the cells were plotted under 0.7 V DC bias at 500 ℃. Figure 3.1(b) displays the spectra.

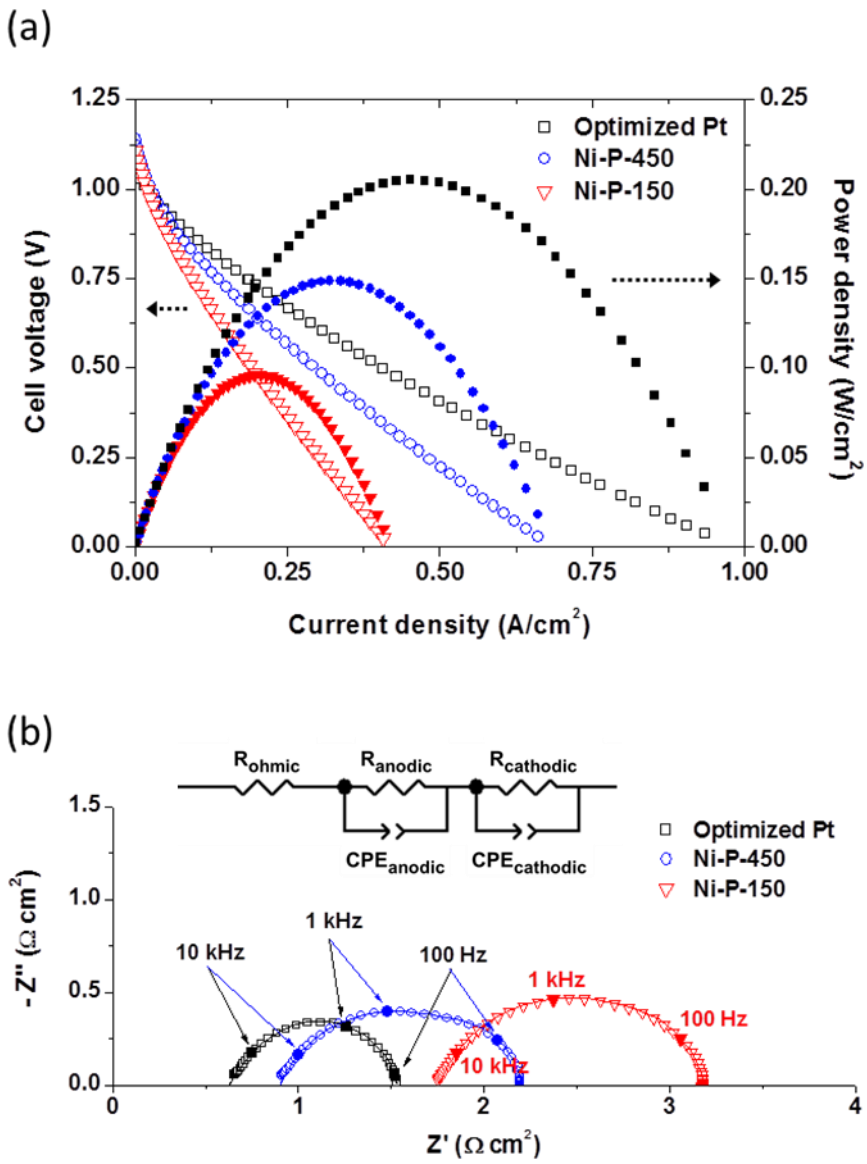

Figure 3.1 (a) j-V-P curves and (b) impedance spectra (under 0.7 V DC bias) of the porous Ni anode cells and the optimized Pt cell at 500 ℃.

In each impedance spectrum, the intersection between the spectrum and the x-axis in the high frequency range usually represents the ohimic resistance. This ohmic resistance mostly comes from the ionic conduction through the electrolyte and the electronic conduction along the electrodes for current collecting process.[3,43-46] On the other hand, the semicircle with a non-zero capacitance of the spectrum represents the polarization resistance, mainly composed of activation and concentration resistances.[3,46-48] The concentration resistance, however, typically increases sharply at the high current density or the low voltage region, resulting in abrupt voltage drop.[3] Since there is no drastic voltage drop in j-V curves, except the low current density region where the activation overvoltage dominantly affects the slope of j-V curves, the semicircles on EIS data would mainly originate from the activation resistances of the cells. Absence of noticeable additional semicircle in the low frequency range of the EIS further substantiates that the influence of the concentration resistance is negligible.[48-50] Therefore, the major factors that vary the size of the semicircle would be anodic and cathodic activation resistances. Since we fabricated the electrolytes and cathodes of Ni-P-150 cell, Ni-P-450 cell, and the optimized Pt cell with identical processes, it is

reasonable to assume that the dominant factors to determine the ohmic resistance and the polarization resistance are the anodic current collecting capability and the catalytic activity of anode, respectively.[28]

For quantitative investigation of the ohmic and polarization resistances, each impedance spectrum was fitted to a basic equivalent circuit as illustrated in Figure 3.1(b). R_{ohmic} indicates the ohmic resistance, while R_{anodic}, CPE_{anodic}, $R_{cathodic}$, and $CPE_{cathodic}$ represent the activation resistances from the anode and the cathode. Measured polarization resistances of Ni-P-150 cell, Ni-P-450 cell, and the optimized Pt cell are 1.42, 1.30, and 0.90 $\Omega \cdot cm^2$, respectively. Although Ni-P-450 cell shows a slightly improved polarization resistance than Ni-P-150 cell, both porous Ni anode cells exhibit significantly larger polarization resistance than the optimized Pt cell. Since we assumed that the anodic activity dominantly affects the polarization resistance, the porous Ni anodes seem to be inferior to the optimized Pt anode in terms of catalytic activity. Moreover, the ohmic resistances of Ni-P-150 cell (1.76 $\Omega \cdot cm^2$) and Ni-P-450 cell (0.90 $\Omega \cdot cm^2$) are also larger than that of the optimized Pt cell (0.63 $\Omega \cdot cm^2$). This indicates that even the thick porous Ni anode cannot provide a sufficient current collecting

capability compared to the optimized Pt anode. Consequently, the porous Ni anodes are not suitable for replacing Pt anodes.

3.1.2. Dense Ni Anodes

After verifying the inferiority of the porous Ni anodes, the dense Ni anodes were examined. Figure 3.2(a) shows the j-V-P curves of the cell with Ni-D-150, the cell with Ni-D-450, and the cell with the optimized Pt anode at 500 ℃. Interestingly, both Ni-D-150 and Ni-D-450 cells exhibit comparable performances to the optimized Pt cell. The peak power densities of the two cells are 196 and 187 mW/cm^2, which correspond to 95.6% and 91.2% of the peak power density of the optimized Pt cell (205 mW/cm^2).

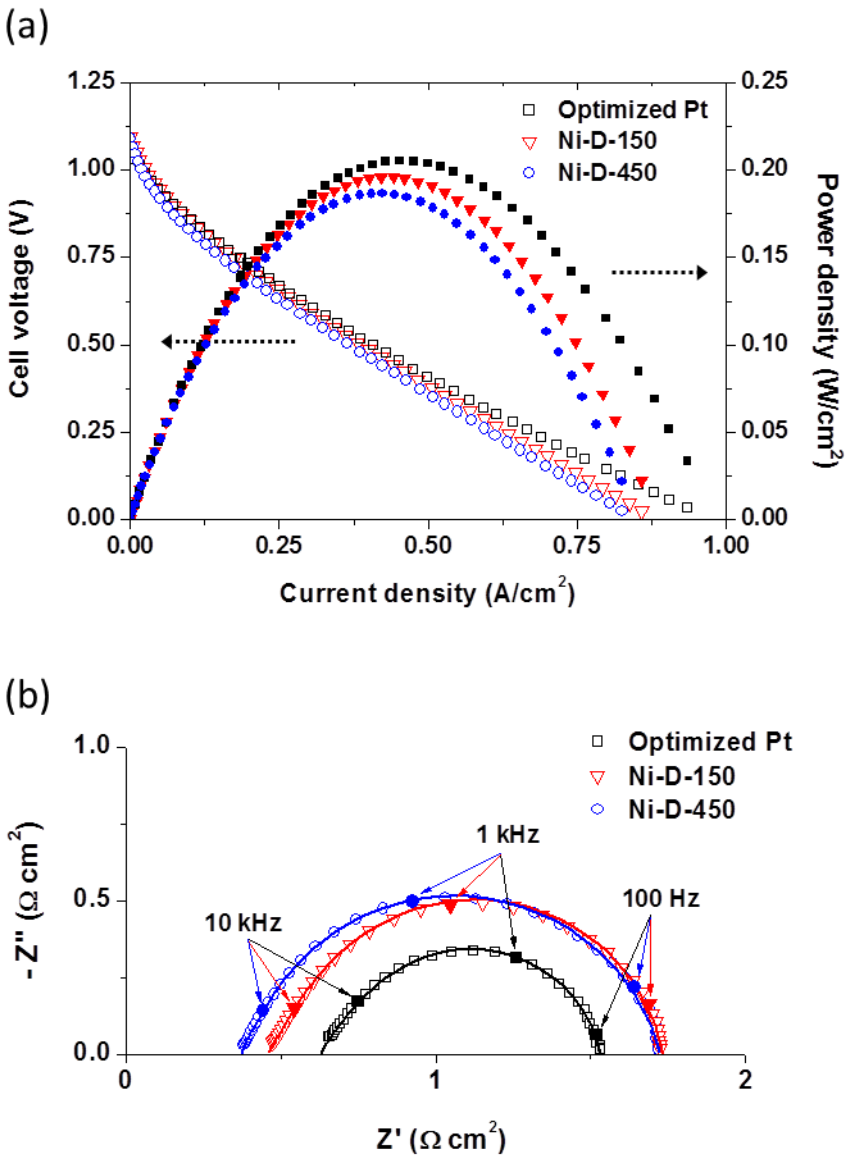

Figure 3.2 (a) j-V-P curves and (b) impedance spectra (under 0.7 V DC bias) of the dense Ni anode cells and the optimized Pt cell at 500 ℃.

From the EIS and fitted EIS data plotted on Figure 3.2(b), the polarization resistances of Ni-D-150 cell, Ni-D-450 cell, and the optimized Pt cell are 1.27, 1.35, and 0.90 $\Omega \cdot cm^2$, while the ohmic resistances of them are 0.46, 0.38, and 0.63 $\Omega \cdot cm^2$, respectively. Both Ni-D-150 and Ni-D-450 cells demonstrate considerably lower ohmic resistance than the optimized Pt cell. Since sputtering at relatively high-degree vacuum condition allows less voids, the dense Ni anodes might have enhanced electrical connection between Ni particles and reduce the anodic current collecting resistance.[41] In addition, relatively thick layer of Ni-D-450 further enhances the electronic conductivity along the anode plane and exhibits the smallest ohmic resistance among the cells.

Although the dense Ni anode cells show low ohmic resistance, their total resistances are still larger than that of the optimized Pt cell because of the higher polarization resistance. Even Ni-D-150 cell, the cell with the smallest polarization resistance among the four Ni anode cells, exhibits approximately 40 % larger polarization resistance than the optimized Pt cell under 0.7 V bias. We speculate that the high polarization resistances of the Ni anodes may come from the different film structure of sputtered Pt and Ni as well as their different catalytic activities. The 450 nm-thick

porous Pt film (optimized Pt anode) consists of diamond-shaped small clusters and voids between those clusters as shown in Figure 3.3. Due to this structure, a large amount of voids can be connected to the pores on AAO template and effectively carry the fuel molecules. Consequently, formation of TPBs can easily occur. On the other hand, Ni films show the larger clusters than the porous Pt film, which form less void boundaries except on the pores from the AAO template. As a result, it is likely that the optimized Pt anode has more TPBs on the anode side than the Ni anodes.

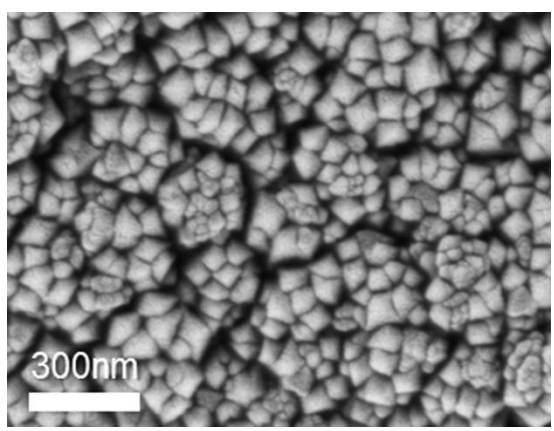

Figure 3.3 Top surface image of the optimized Pt anode

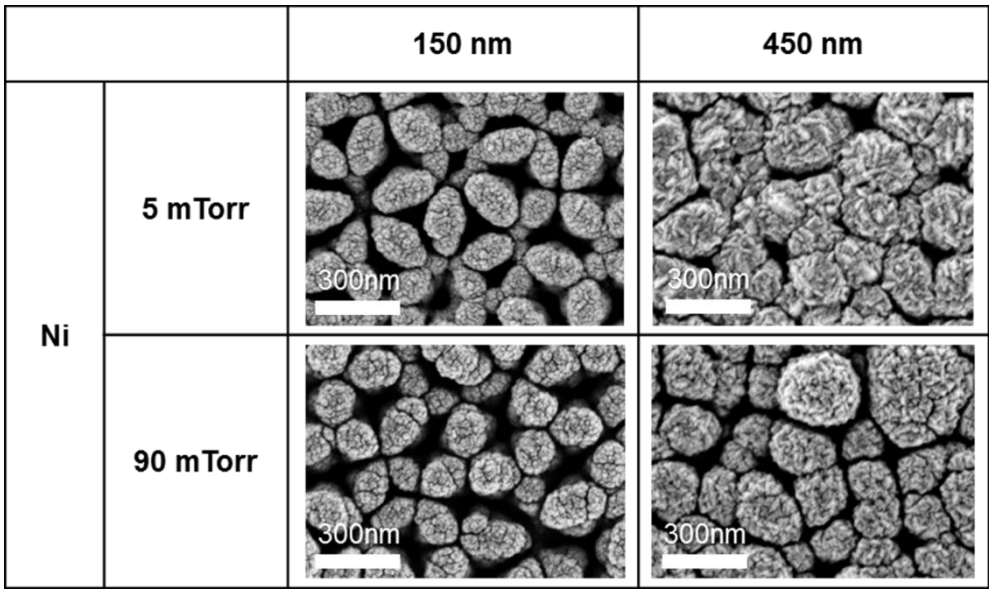

Figure 2.1 Surface morphologies of the fabricated Ni films.

(Copied from Chapter 2 for convenient comparison with Figure 3.3)

As mentioned earlier in 3.1.1., we can assume that the difference in the ohmic resistance comes from the anodic current collecting resistance, whereas the difference in the polarization resistance mainly results from the anodic catalytic activity. Then, we can conclude that all of the Ni anode cells have more sluggish HOR kinetics compared to the optimized Pt cell. Hence, the pure Ni anodes cannot outperform the pure Pt anode in terms of catalytic activity by simple structural modification via sputtering technique.

3.2. Investigating Various Ni-YSZ Anodes

From the results so far, the Ni anodes exhibit relatively sluggish catalytic activity, even though they have better structure for current collecting than the optimized Pt anode. This inferior catalytic activity, however, can be enhanced by enlarging the reaction sites. It has been known that the Ni-YSZ composites increase the TPBs in the electrode/electrolyte interfaces in the powder-based traditional SOFCs.[37,51,52] It is also reported that more than 30 vol% of Ni is required to achieve its percolation for fair electronic conduction, and the maximized catalytic activity can be obtained with the approximately 40 vol% of Ni.[53-56]

In order to increase TPBs in the thin-film Ni-based anodes, we investigated various Ni-YSZ films. For proper operation, the Ni-YSZ film should have both YSZ and Ni percolations in its structure to supply oxygen ions to the reaction sites and collect electrons from there. Hence, an electrochemically favorable Ni-YSZ film shows reasonable electric and ionic conductivities at the same time.[54,55] Figure 3.4 shows the electric conductivities of NY1, NY2, NY3, NY4, and NY5 under room temperature.

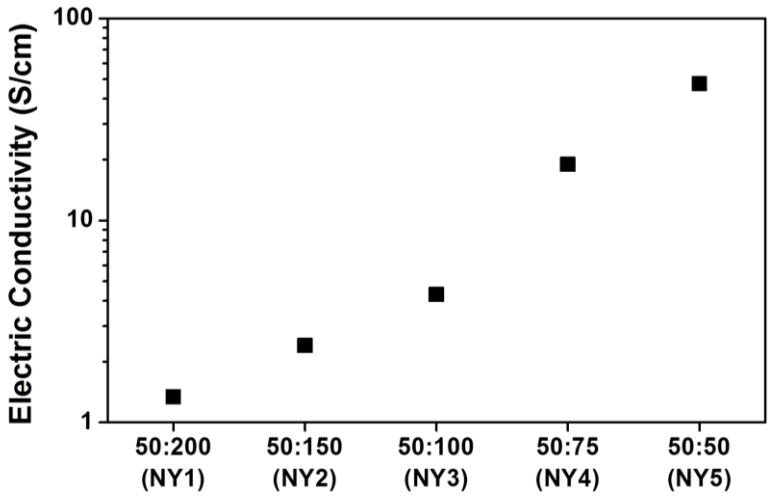

Figure 3.4 Electric conductivities of the Ni-YSZ films under room temperature.

Since the higher RF power accelerates the YSZ sputtering, NY1 would have the highest YSZ and thus the lowest Ni contents among the five films. On the contrary, NY5 would have the highest Ni and the lowest YSZ contents. The electric conductivities of the films fit well with this prediction. As the RF sputtering power decreases, the electric conductivity of the deposited film increases, which indicates that the better Ni connection is constructed throughout the film. It is reasonable to think that the better Ni connection is mainly caused by higher Ni content, since the deposition conditions for Ni sputtering were fixed for the whole Ni-

YSZ film fabrication processes. However, the higher electric conductivity does not guarantee better performance, because the high Ni content can interrupt the formation of YSZ connection and cause the decrease of reaction sites. Consequently, even though NY5 shows the best electric conductivity among the five Ni-YSZ films, it might contain insufficient YSZ percolation which is essential for enlarging TPBs. To obtain more information, we fabricated full cells by utilizing each Ni-YSZ film as an anode layer and measured EIS of the cells under 0.5 V DC bias at 500 ℃. Figure 3.5 illustrates those spectra.

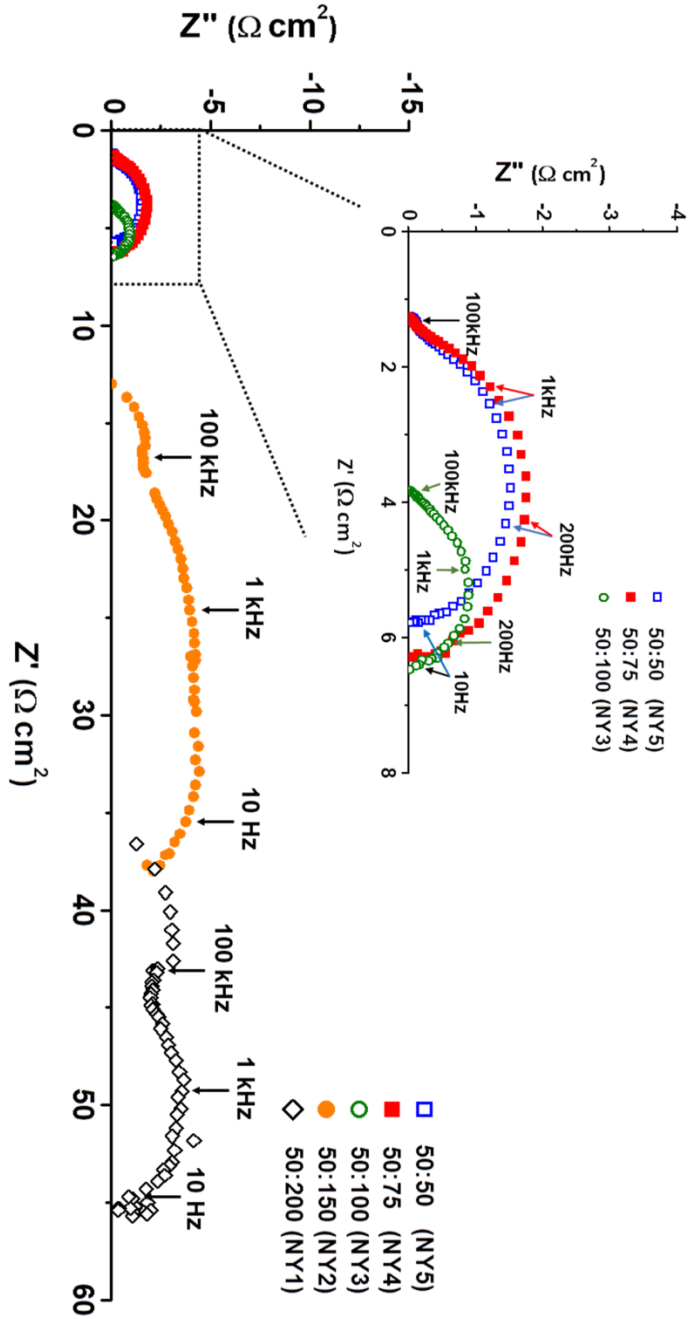

Figure 3.5 Impedance spectra of the various Ni-YSZ anode cells.

From Figure 3.5, NY1 and NY2 cells show extremely high ohmic resistance compared with other cells. Since the ohmic resistance of the film from Figure 3.5 decreases as the RF power increases, the huge ohmic resistance of NY1 and NY2 cells might result from the poor current collecting capability caused by the low Ni content in their anode layers. Since the two cells exhibit not only high ohmic resistance but also significantly large polarization resistance, we concluded that NY1 and NY2 films are not suitable for the anode structure. On the contrary, NY3, NY4, and NY5 cells exhibit relatively fair ohmic and polarization resistances. While NY4 and NY5 cells have similar ohmic and polarization resistances with each other, NY3 cell has considerably low polarization resistance. This may indicate that the NY3 film has the most favorable nanostructure for HOR kinetics. Therefore, we decided to utilize NY3 as an anode functional layer, even though it shows higher ohmic resistance than other two cells.

3.3. Ni/Ni-YSZ Bilayer Anodes

In order to utilize the electrochemically favorable nanostructure of NY3 film while compensating its high ohmic resistance at the same time, we introduced Ni/Ni-YSZ bilayer anode structure. Ni-D-150, the 150 nm-thick dense Ni layer from the section 3.1.2., was selected for the Ni layer due to its good lateral electron collecting capability and wide gas channels. On the AAO, Ni-D-150, a 200 nm-thick layer of NY3 film, a 600 nm-thick YSZ electrolyte, and a 200 nm-thick Pt cathode were deposited sequentially to fabricate a full cell. The full cell was tested at 500 ℃, and Figure 3.6 shows the results.

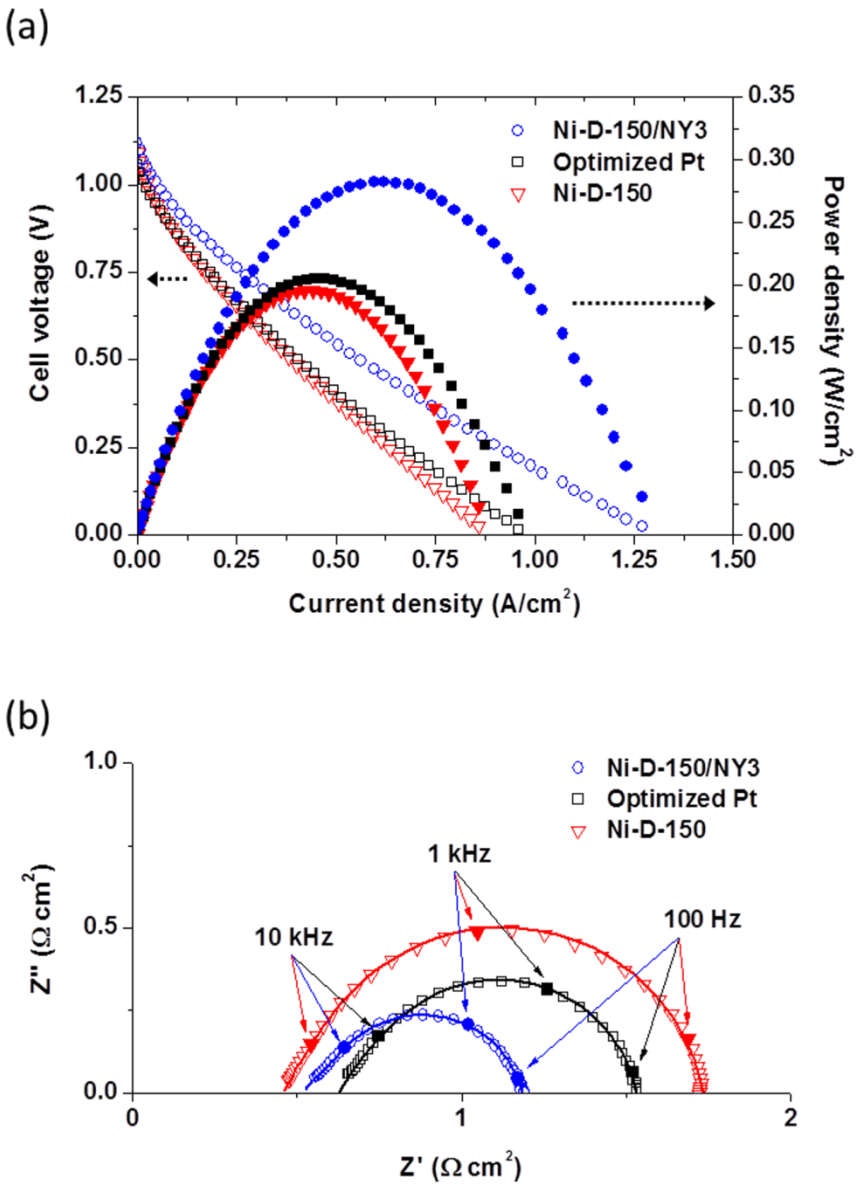

Figure 3.6 (a) j-V-P curves and (b) impedance spectra (under 0.7 V DC bias) of the Ni/Ni-YSZ bilayer cell, Ni-D-150 cell, and the optimized Pt cell at 500 ℃.

As shown in Figure 3.6(a), Ni-D-150/NY3 bilayer anode cell demonstrates remarkably higher performance than Ni-D-150 cell and the optimized Pt cell for the entire current density region. The peak power density of Ni-D-150/NY3 cell, 282 mW/cm^2, is more than 37 % higher than that of the optimized Pt cell. The major reason for this enhancement is the substantial reduction in the polarization resistance of Ni-D-150/NY3 bilayer anode. Figure 3.6(b) shows that the polarization resistance of Ni-D-150/NY3 cell, 0.67 Ω·cm^2, is significantly smaller than that of Ni-D-150 cell, 1.27 Ω·cm^2. This indicates that the Ni-YSZ film significantly increases reaction sites. Additionally, the polarization resistance of Ni-D-150/NY3 cell is even lower than the polarization resistance of the optimized Pt cell, 0.90 Ω·cm^2.

On the other hand, the ohmic resistance of Ni-D-150/NY3 cell (0.52 Ω·cm^2) is smaller than that of the optimized Pt cell (0.63 Ω·cm^2) and slightly higher than that of Ni-D-150 cell (0.46 Ω·cm^2). This suggests that the Ni layer maintains the current collecting capability of the Ni-D-150/NY3 bilayer anode under acceptable range, despite the existence of the cermet layer. The acceptable ohmic resistance of the bilayer cell also shows that the Ni particles in NY3 layer connect to each other properly, so the

electrons from the reaction sites can be transferred to the external circuit. If the Ni percolation was not developed throughout the Ni-YSZ layer, the electric conductivity of the Ni-YSZ layer would considerably decrease and the electrons from the TPBs cannot escape from the electrode/electrolyte interface. This would have an adverse effect on the ohmic resistance and the performance of the cell. In the same way, if the YSZ particles in NY3 layer did not construct ionic percolation, the ionic conductivity of the Ni-YSZ layer would be extremely low and would result in increased ohmic resistance. Therefore, NY3 layer of Ni-D-150/NY3 cell properly acts as a mixed ionic-electronic conductor (MIEC) in our cell as we desired.

Chapter 4. Conclusion

We fabricated several types of pure Ni anodes onto AAO templates to investigate their nanostructure and to utilize them as an anode layer of low-temperature SOFCs. Among the various Ni anodes, the 150 nm-thick Ni anode sputtered under 5 mTorr Ar gas showed highest electrochemical performance. Even though the fuel cell with this Ni anode exhibited comparable performance to the fuel cell with the optimized Pt anode, the optimized Pt anode demonstrated superior polarization resistance to the Ni anode.

In order to enhance the electrochemical characteristics of the Ni anode, we examined five different Ni-YSZ films and compared their electrochemical characteristics. As a result, we selected the co-sputtered film with 50 W DC and 100 W RF powers for an anode functional layer. Then, we fabricated the advanced fuel cell which has AAO/Ni/Ni-YSZ/YSZ/Pt multilayer structure. By inserting the Ni-YSZ composite layer between the Ni anode and YSZ electrolyte, we successfully enhanced the polarization resistance of the cell with Ni-based thin-film anode. Compared to the pure Ni anode cells, the cell with Ni/Ni-YSZ bilayer anode

showed more than 47 % less polarization resistance. In addition, the peak power density of the bilayer anode cell was 282 mW/cm^2 at 500 ℃, about 37 % higher than that of the optimized Pt anode cell. These results indicate that noble metal anodes can be replaced by Ni-based anode in low temperature SOFC applications.

Bibliography

1. Edwards, P. P., Kuznetsov, V. L., David, W. I. F. & Brandon, N. P. Hydrogen and fuel cells: Towards a sustainable energy future. *Energy Policy* **36,** 4356–4362 (2008).
2. Turner, J. A. Sustainable hydrogen production. *Science* **305,** 972–974 (2004).
3. O'hayre, R., Cha, S. W., Colella W. G. & Prinz, F. B. *Fuel Cell Fundamentals, 3rd ed.* John Wiley & Sons, Hoboken, New Jersey (2016)
4. Ormerod, R. M. Solid oxide fuel cells. *Chem. Soc. Rev.* **32,** 17–28 (2003).
5. Haile, S. M. Fuel cell materials and components. *Acta Mater.* **51,** 5981–6000 (2003).
6. Fergus, J. W. Electrolytes for solid oxide fuel cells. *J. Power Sources* **162,** 30–40 (2006).
7. Xin, X., Lü, Z., Ding, Z., Huang, X., Liu, Z., Sha, X., Zhang, Y. & Su, W. Synthesis and characteristics of nanocrystalline YSZ by homogeneous precipitation and its electrical properties. *J. Alloys Compd.* **425,** 69–75 (2006).
8. Guo, X., Vasco, E., Mi, S., Szot, K., Wachsman, E. & Waser, R.

Ionic conduction in zirconia films of nanometer thickness. *Acta Mater.* **53,** 5161-5166 (2005).

9. Wang, S., Kobayashi, T., Dokiya, M. & Hashimoto, T. Electrical and Ionic Conductivity of Gd-Doped Ceria. *J. Electrochem. Soc.* **147,** 3606 (2000).

10. Jud, E. & Gauckler, L. J. The Effect of Cobalt Oxide Addition on the Conductivity of $Ce_{0.9}Gd_{0.1}O_{1.95}$. *J. Electroceramics* **15,** 159-166 (2005).

11. Zhang, T. S., Ma, J., Luo, L. H. & Chan, S. H. Preparation and properties of dense $Ce_{0.9}Gd_{0.1}O_{2-\delta}$ ceramics for use as electrolytes in IT-SOFCs. *J. Alloys Compd.* **422,** 46-52 (2006).

12. Sin, A. Preparation and sintering of $Ce_{1-x}Gd_xO_{2-x/2}$ nanopowders and their electrochemical and EPR characterization. *Solid State Ionics* **175,** 361-366 (2004).

13. Kharton, V. V., Figueiredo, F. M., Navarro, L., Naumovich, E. N., Kovalevsky, A. V., Yaremchenko, A. A., Viskup, A. P., Carneiro, A., Marques, F. M. B. & Frade, J. R. Ceria-based materials for solid oxide fuel cells. *J. Mater. Sci.* **36,** 1105-1117

14. Huang, H., Nakamura, M., Su, P., Fasching, R., Saito, Y. &

Prinz, F. B. High-Performance Ultrathin Solid Oxide Fuel Cells for Low-Temperature Operation. *J. Electrochem. Soc.* **154,** B20-B24 (2007).

15. Steele, B. C. & Heinzel, A. Materials for fuel-cell technologies. *Nature* **414,** 345-352 (2001).

16. Evans, A., Bieberle-Hütter, A., Rupp, J. L. M. & Gauckler, L. J. Review on microfabricated micro-solid oxide fuel cell membranes. *J. Power Sources* **194,** 119-129 (2009).

17. Shao, Z. & Haile, S. M. A high-performance cathode for the next generation of solid-oxide fuel cells. *Nature* **431,** 170-173 (2004).

18. Brandon, N. P., Skinner, S. & Steele, B. C. H. Recent Advances in Materials for Fuel Cells. *Annu. Rev. Mater. Res.* **33,** 183-213 (2003).

19. Noh, H.-S., Son, J.-W., Lee, H., Song, H.-S., Lee, H.-W. & Lee, J.-H. Low Temperature Performance Improvement of SOFC with Thin Film Electrolyte and Electrodes Fabricated by Pulsed Laser Deposition. *J. Electrochem. Soc.* **156,** B1484-B1490 (2009).

20. Myung, D.-H., Hong, J., Yoon, K., Kim, B.-K., Lee, H.-W., Lee, J.-H. & Son, J.-W. The effect of an ultra-thin zirconia

blocking layer on the performance of a 1-μm-thick gadolinia-doped ceria electrolyte solid-oxide fuel cell. *J. Power Sources* **206,** 91-96 (2012).

21. Shim, J. H., Kang, S., Cha, S.-W., Lee, W., Kim, Y. B., Park, J. S., Gür, T. M., Prinz, F. B., Chao, C.-C. & An, J. Atomic layer deposition of thin-film ceramic electrolytes for high-performance fuel cells. *J. Mater. Chem. A* **1,** 12695-12705 (2013).

22. An, J., Kim, Y.-B., Park, J., Gür, T. M. & Prinz, F. B. Three-dimensional nanostructured bilayer solid oxide fuel cell with 1.3 W/cm(2) at 450 ° C. *Nano Lett.* **13,** 4551-5 (2013).

23. Su, P.-C., Chao, C.-C., Shim, J. H., Fasching, R. & Prinz, F. B. Solid oxide fuel cell with corrugated thin film electrolyte. *Nano Lett.* **8,** 2289-2292 (2008).

24. Shim, J. H., Chao, C.-C., Huang, H. & Prinz, F. B. Atomic Layer Deposition of Yttria-Stabilized Zirconia for Solid Oxide Fuel Cells. *Chem. Mater.* **19,** 3850-3854 (2007).

25. Baek, J. D., Yoon, Y.-J., Lee, W. & Su, P.-C. A circular membrane for nano thin film micro solid oxide fuel cells with enhanced mechanical stability. *Energy Environ. Sci.* **8,** 3374-3380 (2015).

26. Ji, S., Cho, G. Y., Yu, W., Su, P.-C., Lee, M. H. & Cha, S. W. Plasma-enhanced atomic layer deposition of nanoscale yttria-stabilized zirconia electrolyte for solid oxide fuel cells with porous substrate. *ACS Appl. Mater. Interfaces* **7,** 2998-3002 (2015).

27. Cho, G. Y., Noh, S., Lee, Y. H., Ji, S., Hong, S. W., Koo, B., An, J., Kim, Y.-B. & Cha, S. W. Properties of nanostructured undoped ZrO_2 thin film electrolytes by plasma enhanced atomic layer deposition for thin film solid oxide fuel cells. *J. Vac. Sci. Technol. A Vacuum, Surfaces, Film.* **34,** 01A151-01A151-7 (2016).

28. Park, J., Lee, Y., Chang, I., Lee, W. & Cha, S. W. Engineering of the electrode structure of thin film solid oxide fuel cells. *Thin Solid Films* **584,** 125-129 (2015).

29. Chang, I., Bae, J., Park, J., Lee, S., Ban, M., Park, T., Lee, Y. H., Song, H. H., Kim, Y.-B. & Cha, S. W. A thermally self-sustaining solid oxide fuel cell system at ultra-low operating temperature (319 ℃). *Energy* **104,** 107-113 (2016).

30. Park, Y., Su, P. C., Cha, S. W., Saito, Y. & Prinz, F. B. Thin-Film SOFCs Using Gastight YSZ Thin Films on Nanoporous Substrates. *J. Electrochem. Soc.* **153,** A431-A436 (2006).

31. Kang, S., Su, P. C., Park, Y. I., Saito, Y. & Prinz, F. B. Thin-Film Solid Oxide Fuel Cells on Porous Nickel Substrates with Multistage Nanohole Array. *J. Electrochem. Soc.* **153,** A554-A559 (2006).

32. Calle-Vallejo, F., Koper, M. T. M. & Bandarenka, A. S. Tailoring the catalytic activity of electrodes with monolayer amounts of foreign metals. *Chem. Soc. Rev.* **42,** 5210-5230 (2013).

33. Trasatti, S. Work function, electronegativity, and electrochemical behaviour of metals. *J. Electroanal. Chem. Interfacial Electrochem.* **39,** 163-184 (1972).

34. Quaino, P., Juarez, F., Santos, E. & Schmickler, W. Volcano plots in hydrogen electrocatalysis – uses and abuses. *Beilstein J. Nanotechnol.* **5,** 846-854 (2014).

35. Wendt, H., Spinacé, E. V., Oliveira Neto, A. & Linardi, M. Electrocatalysis and electrocatalysts for low temperature fuel cells: fundamentals, state of the art, research and development. *Quim. Nova* **28,** 1066-1075 (2005).

36. Shearing, P. R., Brett, D. J. L. & Brandon, N. P. Towards intelligent engineering of SOFC electrodes: a review of advanced microstructural characterisation techniques. *Int.*

Mater. Rev. **55,** 347–363 (2010).

37. Virkar, A. The role of electrode microstructure on activation and concentration polarizations in solid oxide fuel cells. *Solid State Ionics* **131,** 189–198 (2000).

38. Park, J., Chang, I., Paek, J. Y., Ji, S., Lee, W., Cha, S. W. & Lee, J.-M. Fabrication of the large area thin-film solid oxide fuel cells. *CIRP Ann. - Manuf. Technol.* **63,** 513–516 (2014).

39. Noh, S., Cho, G. Y., Lee, Y. H., Yu, W., An, J. & Cha, S. W. Performance Enhancement in Thin Film Solid Oxide Fuel Cells Using Metal-Mixed Ionic Electronic Conductors Bilayer Anode. *Sci. Adv. Mater.* **8,** 11–16 (2016).

40. Park, J. H. Han, S. M., Yoon, K. J., Kim, H., Hong, J., Kim, B.-K., Lee, J.-H. & Son, J.-W. Impact of nanostructured anode on low-temperature performance of thin-film-based anode-supported solid oxide fuel cells. *J. Power Sources* **315,** 324–330 (2016).

41. Geetha Priyadarshini, B., Aich, S. & Chakraborty, M. Structural and morphological investigations on DC-magnetron-sputtered nickel films deposited on Si (100). *J. Mater. Sci.* **46,** 2860–2873 (2010).

42. Chang, I., Woo, S., Lee, M. H., Shim, J. H., Piao, Y. & Cha, S.

W. Characterization of porous Pt films deposited via sputtering. *Appl. Surf. Sci.* **282,** 463–466 (2013).

43. McIntosh, S., Vohs, J. M. & Gorte, R. J. Impedance Spectroscopy for the Characterization of Cu–Ceria–YSZ Anodes for SOFCs. *J. Electrochem. Soc.* **150,** A1305–A1312 (2003).

44. Fu, C., Sun, K., Zhang, N., Chen, X. & Zhou, D. Electrochemical characteristics of LSCF–SDC composite cathode for intermediate temperature SOFC. *Electrochim. Acta* **52,** 4589–4594 (2007).

45. Leonide, A., Apel, Y. & Ivers–Tiffee, E. SOFC Modeling and Parameter Identification by Means of Impedance Spectroscopy. *ECS Transactions* **19,** 81–109 (2009).

46. Huang, Q.–A., Hui, R., Wang, B. & Zhang, J. A review of AC impedance modeling and validation in SOFC diagnosis. *Electrochim. Acta* **52,** 8144–8164 (2007).

47. Wagner, N., Schnurnberger, W., Müller, B. & Lang, M. Electrochemical impedance spectra of solid–oxide fuel cells and polymer membrane fuel cells. *Electrochim. Acta* **43,** 3785–3793 (1998).

48. Barfod, R., Mogensen, M., Klemensø, T., Hagen, A., Liu, Y.–L.

& Hendriksen, P. V. Detailed Characterization of Anode-Supported SOFCs by Impedance Spectroscopy. *J. Electrochem. Soc.* **154,** B371-B378 (2007).

49. Primdahl, S. Gas Diffusion Impedance in Characterization of Solid Oxide Fuel Cell Anodes. *J. Electrochem. Soc.* **146,** 2827-2833 (1999).

50. DiGiuseppe, G. & Sun, L. Electrochemical performance of a solid oxide fuel cell with an LSCF cathode under different oxygen concentrations. *Int. J. Hydrogen Energy* **36,** 5076-5087 (2011).

51. Costamagna, P., Costa, P. & Antonucci, V. Micro-modelling of solid oxide fuel cell electrodes. *Electrochim. Acta* **43,** 375-394 (1998).

52. Sun, C. & Stimming, U. Recent anode advances in solid oxide fuel cells. *J. Power Sources* **171,** 247-260 (2007).

53. Dees, D. W. Conductivity of Porous Ni/ZrO_2-Y_2O_3 Cermets. *J. Electrochem. Soc.* **134,** 2141-2146 (1987).

54. Koide, H. Properties of Ni/YSZ cermet as anode for SOFC. *Solid State Ionics* **132,** 253-260 (2000).

55. Vivet, N., Chupin, S., Estrade, E., Richard, A., Bonnamy, S., Rochais, D. & Bruneton, E. Effect of Ni content in SOFC Ni-

YSZ cermets: A three-dimensional study by FIB-SEM tomography. *J. Power Sources* **196,** 9989-9997 (2011).

56. Lee, J. Quantitative analysis of microstructure and its related electrical property of SOFC anode, Ni-YSZ cermet. *Solid State Ionics* **148,** 15-26 (2002).

국 문 초 록

본 연구는 저온에서 작동하는 박막 고체산화물 연료전지에 적용할 수 있는 저가형 연료극을 개발하고, 이를 이용하여 고가의 촉매 물질을 대체하고자 진행되었다. 이를 위해, 다양한 구조의 순수 니켈 및 니켈 기반 세르멧 전극과 이를 활용한 연료전지가 제작되었다. 연료전지 제작에는 나노 다공성의 양극 산화 알루미늄 기판 위에 연료극, 전해질, 공기극을 차례대로 증착하는 방법이 사용되었다.

순수 니켈로 만들어진 연료극의 경우, 500 ℃ 조건에서 전극의 나노구조에 따라 백금 연료극에도 크게 뒤쳐지지 않는 성능을 나타냈다. 특히, 5 mTorr 아르곤 환경에서 DC 200 W 전력으로 증착한 150 nm 두께의 순수 니켈 연료극은 이전 연구에서 가장 좋은 성능을 보였던 백금 연료극에 준하는 성능을 보였다. 그러나, 백금 연료극에 비해 집전 저항 측면에서 강점을 보였던 것이지, 더 나은 전극 반응성을 가진 것은 아니었다. 최적화된 백금 연료극을 사용한 연료전지와 니켈 연료극을 이용한 연료전지는 반응저항 측면에서 상당히 큰 차이를 보였고, 따라서 스퍼터링을 활용한 단순 구조변화만으로는 백금 연료극의 반응성을 넘어서기 어렵다고 판단하였다.

니켈 기반 연료극의 반응성을 향상시켜 더 나은 전기화학적 특성을 가지도록 만들기 위해, 니켈/니켈 기반 세르멧 이층층 연료극 구조를 도입하였다. 전기전도도와 이온전도도를 동시에 가지는 세르멧

물질은 전자전도체, 이온전도체, 공극이 모두 함께 존재해야 형성될 수 있는 전기화학 반응점인 삼상계면을 극대화하기에 좋은 것으로 알려져 있다. 다만, 세르멧 물질은 조성비에 따라 그 특성이 크게 변하기 때문에, 전기화학적 촉매로 사용하기에 최적화된 조성비를 찾아야만 한다. 이를 찾고자, 다섯 가지 종류의 니켈-이트리아 안정화 지르코니아 세르멧 박막이 제작되었다. 세르멧 박막의 제작에는 코스퍼터링 공정이 사용되었는데, 모든 세르멧 박막 제작에 있어서 니켈 타겟의 스퍼터링 전력은 DC 50 W로 고정시킨 반면, 이트리아 안정화 지르코니아 타겟의 스퍼터링 전력은 각각 RF 50, 75, 100, 150, 200 W로 다르게 하여 조성비에 변화를 주었다. 제작된 세르멧 박막 중, DC 50 W와 RF 100 W 조건으로 코스퍼터링하여 제작한 박막이 가장 좋은 전극 반응성을 보였다. 때문에, 이 조건의 세르멧 박막을 200 nm 두께로 제작하여 니켈/니켈-이트리아 안정화 지르코니아 이중층 연료극을 만들기로 결정하였다. 순수 니켈 층으로는 표면에 많은 공극을 가지고 있고, 제작한 순수 니켈 박막 중에서 가장 좋은 성능을 보였던 5mTorr 아르곤 환경에서 DC 200 W 전력으로 증착한 150 nm 두께의 니켈 박막을 선택하였다.

선택된 순수 니켈 층과 니켈-이트리아 안정화 지르코니아 세르멧 층을 포함한 이중층 연료극을 가진 연료전지는 500 ℃ 조건에서 282 mW/cm^2의 최대전력밀도를 보였다. 이는 이전 연구에서 가장 좋은 성능을 보였던 백금 연료극 기반 연료전지의 최대전력밀도(205

W/cm^2)보다도 37 % 이상 높은 값으로, 값싼 니켈 기반 전극이 박막과 저온 작동 조건에서도 고가의 촉매물질을 대체할 수 있다는 가능성을 보여주었다. 최대전력밀도뿐 아니라, 세부지표인 옴 저항과 전극저항도 타 연료극을 가진 연료전지에 비해 훨씬 낮은 값을 보였다.

저온 박막 고체산화물 연료전지는 고정형 전원장치에만 한정되어있던 고체산화물 연료전지의 적용범위를 이동형 전원장치로 확대할 수 있다는 점에서 매우 큰 파급효과를 가진다. 그러나, 온도가 낮아짐에 따라 촉매의 반응성이 급격하게 떨어지기 때문에 고가의 촉매를 사용해야 하는 등, 실제 사용 가능한 전원장치로 제작하기에는 많은 어려움이 따르고 있다. 본 연구에서 연료극 구조의 변화를 통해 저가형 전극의 저온 작동 가능성을 확인하였으므로, 앞으로의 저온 박막 고체산화물 연료전지 개발에 큰 도움이 되기를 기대한다.

주요어 : 고체산화물 연료전지, 박막, 저온 작동, 니켈-이트리아 안정화 지르코니아, 코스퍼터링

학 번 : 2014-21866